SAMPLED-DATA CONTROL OF DUAL-ACTIVE BRIDGE DC-DC CONVERTERS WITH TIME DELAY

Khanh Hieu Nguyen[1], Tien Dung Le[2*]

[1]*Department of Convergence Engineering for Intelligent Drone, Sejong University, Seoul 05006, Korea*
[2]*The University of Danang - University of Science and Technology, Danang 550000, Vietnam*

*Corresponding author: ltdung@dut.udn.vn

(Received: April 29, 2025; Revised: June 16, 2025; Accepted: June 19, 2025)

DOI: 10.31130/ud-jst.2025.23(10B).647E

Abstract - This paper addresses the design of a networked control system for dual-active bridge (DAB) DC-DC converters to track a prescribed output-voltage reference. Specifically, it tackles two primary challenges: the sampled-data control problem and time delay issues arising from networked communication. To this end, a mathematical model of the DAB DC-DC converter is formulated as a linear state-space system. Subsequently, an improved looped-functional and an additional discontinuous function are incorporated into the time-dependent Lyapunov function. Accordingly, sufficient stability and stabilization conditions are derived in the form of linear matrix inequalities (LMIs). Finally, simulation results are presented to validate the effectiveness of the proposed method.

Key words - Sampled-data control; dual-active-bridge DC–DC converters; time delay

1. Introduction

Dual-active bridge DC-DC converters are widely recognized as essential power electronic devices capable of facilitating bidirectional energy transfer between two direct current voltage sources. Due to their high efficiency and operational flexibility, DAB DC-DC converters have been extensively deployed across diverse application domains, including consumer electronics, renewable energy systems, energy storage infrastructures, and automotive power systems (refer to [1], [2]). Meanwhile, recent technological advancements have increasingly directed attention towards digital networked control systems within the field of control systems [3], [4]. Among the various approaches explored, sampled-data control has emerged as a particularly effective method for managing networked control systems by discretizing control input updates at specific time intervals rather than maintaining continuous updates, sampled-data control significantly reduces the demands on both communication and computational resources (see [5] - [7]).

In this context, numerous digital control strategies have been developed for DAB DC-DC converters. For instance, the work presented in [8] introduced a bilinear discrete-time model that characterizes the converter dynamics through four distinct switching states within a single switching cycle. Building upon this model, the study in [9] utilized discrete-time modeling combined with a linearized control framework to design a digital controller for DAB DC-DC converters. Further developments were reported in [10], where both large-signal and small-signal discrete-time models were formulated using a time-scale analytical approach. More recently, [11] proposed a model predictive control scheme incorporating a novel parameter identification technique alongside a moving discretization strategy.

Despite significant advancements in digital control design for DAB DC-DC converters, most existing strategies remain predominantly based on discrete-time modeling frameworks. However, there approaches may prove insufficient in accurately capturing dynamic behavior, particularly under conditions of extended sampling intervals. This paper aims to develop a sampled-data control strategy for DAB DC-DC converters with time delay subject to maximizing the allowable sampling interval. Especially, to effectively utilize the information embedded in system state responses during the sampling and transmission processes, an improved looped-functional and a discontinuous function were incorporated into the stability analysis.

Notations: Throughout this paper, $\mathbb{N}$, $\mathbb{N}_0$, and $\mathbb{R}_{n\times n}$ stand for sets of positive natural numbers, natural numbers including zero, and all n $\times n$ real matrices, respectively. For any square matrix Q, notation Q^{-1} indicates the inverse of Q, Q^T is the transpose of Q, and $He\{\mathrm{Q}\}$ stands for $\mathrm{Q} + Q^T$. In symmetric block matrices, the symbol $(*)$ is used to represent terms induced by symmetry. The operator $\otimes$ indicates the Kronecker product. The notation I_n denotes the n-dimensional identity matrix, $0_{m\times n}$ denotes the m $\times n$ zero matrix, $diag\{\cdot\}$ stands for the block-diagonal matrix, and $col\{\cdot\}$ indicates the column matrix.

2. Problems statement

2.1. System description

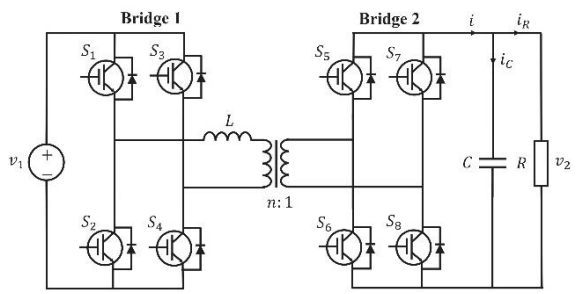

Figure 1. *Model of DAB DC-DC converter*

Figure 1 presents the circuit configuration of the DAB DC-DC converter investigated in this study. The system consists of four pairs of power switches(S_1, S_2), (S_3, S_4), (S_5, S_6), and (S_7, S_8) each operating in a complementary

manner. The inductance L accounts for both the external inductance and the transformer's leakage inductance, while n denotes the transformer turns ratio. The output-side capacitance is represented by C, and the load resistance is denoted by R. The variables $\mathrm{i}(t)$, $i_C(t)$, and $i_R(t)$ represent the output current, capacitor current, and measurable load current, respectively. The input voltage v_1 is given, whereas the output voltage $v_2(t)$ is measurable. Then, the transferred power is given as (see [12]):

$$p(t) = \frac{nv_1v_2(t)}{2f_sL}(1 - |d(t)|)d(t) \tag{1}$$

where $\mathrm{d}(t) \in [-0.5,\ 0.5]$ denotes the phase shift ratio, and f_s represents the switching frequency. Furthermore, since $\mathrm{p}(t) = v_2(t)\mathrm{i}(t)$, it follows that

$$i(t) = \frac{nv_1}{2f_sL}u_d(t) \tag{2}$$

where $u_d(t) = \mathrm{d}(t)(1 - |d(t)|) \in [-0.25,\ 0.25]$. Then, by applying Kirchhoff's current law, we have

$$C\dot{v}_2(t) = i(t) - i_R(t). \tag{3}$$

Thus, from (2), (3), and $i_R(t) = v_2(t)/\mathrm{R}$, it follows that

$$\dot{v}_2(t) = \theta_1 v_2(t) + \theta_2 u_d(t) \tag{4}$$

where

$$\theta_1 = -\frac{1}{RC},\ \theta_2 = \frac{nv_1}{2f_sLC}.$$

From (4), the steady-state value of $u_d(t)$ is given as:

$$u_d^* = \frac{2f_sL}{nv_1R}v_2^{ref} \tag{5}$$

where v_2^{ref} denotes the reference value of $v_2(t)$. Subsequently, by defining $x_1(t) = v_2(t) - v_2^{ref}$ and $x_2(t) = \int_0^t \left(v_2(\mathrm{s}) - v_2^{\mathrm{ref}}\right)ds$, it is given from (4) that

$$\begin{cases} \dot{x}_1(t) = \theta_1\, x_1(t) + \theta_2 u(t) \\ \dot{x}_2(t) = x_1(t) \end{cases} \tag{6}$$

where $\mathrm{u}(t) = u_d(t) - u_d^*$. Therefore, the DAB DC-DC converter can be represented by the following linear state-space model:

$$\dot{x}(t) = Ax(t) + Bu(t) \tag{7}$$

where $\mathrm{x}(t) = \mathrm{col}\{x_1(t), x_2(t)\}$ and

$$\mathrm{A} = \begin{bmatrix} \theta_1 & 0 \\ 1 & 0 \end{bmatrix},\ \mathrm{B} = \begin{bmatrix} \theta_2 \\ 0 \end{bmatrix}.$$

2.2. Controller design

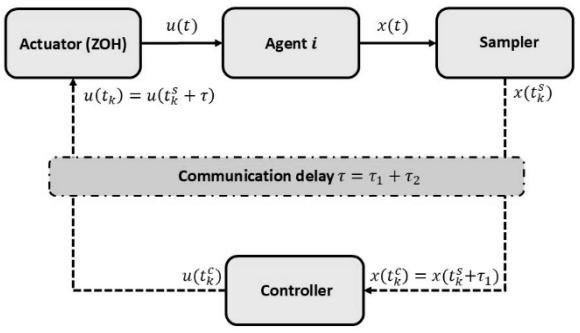

Figure 2. *Diagram of sampled-data controller with time delay*

As illustrated in Figure 2, the system states are sampled at discrete time instants t_k^s, for $\mathrm{k} \in \mathbb{N}_0$, and subsequently transmitted over a communication network with transmission delays τ_1 and τ_2. Accordingly, the sampled state is received by the controller at $t_k^c = t_k^s + \tau_1$, and the corresponding control input is delivered to the actuator at $t_k = t_k^s + \tau_1 + \tau_2 = t_k^s + \tau$, where τ denotes the total communication delay. In addition, the time interval between two consecutive samplings $h_k = t_{k+1}^s - t_k^s = t_{k+1} - t_k \in [h_m, h_M]$. Then, the sampled-data control input is given as:

$$u(t) = Fx(t_k^s) = Fx(t_k - \tau), \forall t \in [t_k, t_{k+1}) \tag{8}$$

where F denotes the controller gain. Then, the closed-loop system with (7) and (8) is rewritten as:

$$\dot{x}(t) = Ax(t) + BFx(t_k - \tau). \tag{9}$$

3. Stabilization criterion

For the sake of brevity, the following notational are introduced: $d_1(t) = \mathrm{t} - t_k$, $d_2(t) = t_{k+1} - \mathrm{t}$, $\tau_M = \tau + h_M$, and

$$\eta(t) = col\left\{x(t),\, x(t-\tau),\, x(t_k - \tau),\, x(t_{k+1} - \tau),\, \int_{t_k-\tau}^{t-\tau} x(s)ds,\, \int_{t-\tau}^{t_{k+1}-\tau} x(s)\, ds,\, \dot{x}(t), \dot{x}(t-\tau)\right\}$$

$$\eta_{\mathrm{j}}(t) = \Xi_{\mathrm{j}}\eta(t),\ \dot{\eta}_j(t) = \bar{\Xi}_j\eta(t),\ \eta_{\mathrm{j}}(t-\tau) = \hat{\Xi}_j\eta(t).$$

The following theorem presents the stability condition for closed loop system (9) for given control gain.

Theorem 1: For given positive scalars ε_1, ε_2, τ, h_m, and h_M, the closed-looped system (9) is asymptotically stable, if there exist matrices $0 < P = P^T \in \mathbb{R}^{n\times n}$, $0 < W = W^T \in \mathbb{R}^{2n\times 2n}$, $0 < S = S^T \in \mathbb{R}^{n\times n}$, X_1, $X_2 \in \mathbb{R}^{2n\times 3n}$, $R_1 = R_1^T$, $R_2 = R_2^T \in \mathbb{R}^{n\times n}$, $U = U^T \in \mathbb{R}^{2n\times 2n}$, $Q_1 = Q_1^T \in \mathbb{R}^{2n\times 2n}$, $Q_2 \in \mathbb{R}^{n\times 2n}$, $Q_3 = Q_3^T \in \mathbb{R}^{n\times n}$, and $G \in \mathbb{R}^{n\times n}$ such that the following conditions are satisfied, for $h_k \in \{h_m, h_M\}$:

$$0 < \begin{bmatrix} \mathrm{Q}_1 & (*) \\ \mathrm{Q}_2 & \mathrm{Q}_3 \end{bmatrix} \tag{10}$$

$$0 > \begin{bmatrix} \Psi_1 + \Psi_2(\mathrm{t_k}) & (*) & (*) \\ \tau \mathrm{M}\Xi_8 & -\tau\, \mathrm{S} & 0 \\ \mathrm{h_k N_2}\Xi_{10} & 0 & -\mathrm{h_k R_2} \end{bmatrix} \tag{11}$$

$$0 > \begin{bmatrix} \Psi_1 + \Psi_2(\mathrm{t_{k+1}}) & (*) & (*) \\ \tau \mathrm{M}\Xi_8 & -\tau\, \mathrm{S} & 0 \\ \mathrm{h_k N_1}\Xi_9 & 0 & -\mathrm{h_k R_1} \end{bmatrix} \tag{12}$$

where

$$\begin{aligned} \Psi_1 = {} & He\{\boldsymbol{e}_1^T P \boldsymbol{e}_7\} + \Xi_1^T \mathrm{W}\Xi_1 - \hat{\Xi}_1^T \mathrm{W}\hat{\Xi}_1 + \tau \boldsymbol{e}_7^T \mathrm{S}\boldsymbol{e}_7 \\ & + He\{(\boldsymbol{e}_1^T - \boldsymbol{e}_2^T)M\Xi_8 + (\boldsymbol{e}_2^T - \boldsymbol{e}_3^T)N_1\Xi_9\} \\ & + He\{(\boldsymbol{e}_4^T - \boldsymbol{e}_2^T)N_2\Xi_{10} - \Xi_2^T X_1 \Xi_3 + \Xi_4^T X_2 \Xi_5\} \\ & + He\{\Xi_{11}^T G^T (A\boldsymbol{e}_1 + BF\boldsymbol{e}_3 - \boldsymbol{e}_7) + \tau_M \bar{\Xi}_7^T Q_1 \Xi_7\} \\ & + He\{\boldsymbol{e}_8^T Q_2 \Xi_7 + (\boldsymbol{e}_2^T - \boldsymbol{e}_3^T)Q_2\bar{\Xi}_7 + \boldsymbol{e}_8^T Q_3 \boldsymbol{e}_8\} \end{aligned}$$

$$\begin{aligned} \Psi_2(t) = {} & d_2(t) He\{\bar{\Xi}_2^T X_1 \Xi_3 + \Xi_2^T X_1 \bar{\Xi}_3 + \Xi_6^T U \Xi_6 + \boldsymbol{e}_8^T R_1 \boldsymbol{e}_8\} \\ & + d_1(t) He\{\bar{\Xi}_4^T X_2 \Xi_5 + \Xi_4^T X_2 \bar{\Xi}_5 - \Xi_6^T U \Xi_6 + \boldsymbol{e}_8^T R_2 \boldsymbol{e}_8\} \end{aligned}$$

in which

$\Xi_1 = col\{\boldsymbol{e}_1, \boldsymbol{e}_7\}, \hat{\Xi}_1 = \mathrm{col}\{\boldsymbol{e}_2, \boldsymbol{e}_8\}$
$\Xi_2 = col\{\boldsymbol{e}_2 - \boldsymbol{e}_3, \boldsymbol{e}_5\}, \Xi_3 = \mathrm{col}\{\boldsymbol{e}_2, \boldsymbol{e}_3, \boldsymbol{e}_5\}$
$\Xi_4 = col\{\boldsymbol{e}_4 - \boldsymbol{e}_2, \boldsymbol{e}_6\}, \Xi_5 = \mathrm{col}\{\boldsymbol{e}_2, \boldsymbol{e}_4, \boldsymbol{e}_6\}$
$\bar{\Xi}_2 = col\{\boldsymbol{e}_8, \boldsymbol{e}_2\}, \bar{\Xi}_3 = col\{\boldsymbol{e}_8, 0, \boldsymbol{e}_2\}$
$\bar{\Xi}_4 = col\{-\boldsymbol{e}_8, -\boldsymbol{e}_2\}, \bar{\Xi}_5 = col\{\boldsymbol{e}_8, 0, -\boldsymbol{e}_2\}$
$\Xi_6 = col\{\boldsymbol{e}_3, \boldsymbol{e}_4\}, \Xi_7 = col\{\boldsymbol{e}_2, \boldsymbol{e}_3\}, \bar{\Xi}_7 = col\{\boldsymbol{e}_8, 0\}$
$\Xi_8 = col\{\boldsymbol{e}_1, \boldsymbol{e}_2\}, \Xi_9 = col\{\boldsymbol{e}_2, \boldsymbol{e}_3\}, \Xi_{10} = col\{\boldsymbol{e}_2, \boldsymbol{e}_4\}$
$\Xi_{11} = \boldsymbol{e}_1 + \varepsilon_1 \boldsymbol{e}_3 + \varepsilon_2 \boldsymbol{e}_7$
$\boldsymbol{e}_i = [0_{n\times(i-1)n}\ I_n\ 0_{n\times(8-i)n}]$.

Proof: We construct the following Lyapunov–Krasovskii functional (LKF):

$$V(t) = V_1(t) + V_2(t) + V_3(t), \forall t \in [t_k, t_{k+1}) \quad (13)$$

where

$$\begin{aligned}
V_1(t) &= x^T(t)Px(t) + \int_{t-\tau}^{t} \eta_1^T(s) W \eta_1(s) ds \\
&\quad + \int_{-\tau}^{0}\int_{t+\sigma}^{t} \dot{x}^T(s) S \dot{x}(s) d\, s d\sigma \\
V_2(t) &= 2d_2(t)\eta_2^T(t)X_1\eta_3(t) + 2d_1(t)\eta_4^T(t)X_2\eta_5(t) \\
&\quad + d_2(t)\int_{t_k-\tau}^{t-\tau} \dot{x}^T(s)R_1\dot{x}(s)ds \\
&\quad - d_1(t)\int_{t-\tau}^{t_{k+1}-\tau} \dot{x}^T(s)R_2\dot{x}(s)ds \\
&\quad + d_1(t)d_2(t)\eta_6^T U \eta_6 \\
V_3(t) &= \tau_M \eta_7^T(t)Q_1\eta_7(t) \\
&\quad + 2\big(x^T(t-\tau) - x^T(t_k-\tau)\big)Q_2\eta_7(t) \\
&\quad + \int_{t_k-\tau}^{t-\tau} \dot{x}^T(s)Q_3\dot{x}(s)ds.
\end{aligned}$$

Remark 1: Since $V_2(t_k) = 0$ and $\lim_{t\to t_{k+1}^-} V_2(t) = 0$, the positive definiteness of $V_2(t)$ can be omitted according to the looped-functional approach [5]. Then, condition (10) ensures that

$$0 < \int_{t_k-\tau}^{t-\tau} \begin{bmatrix}\eta_7(t)\\ \dot{x}(s)\end{bmatrix}^T \begin{bmatrix}Q_1 & (*)\\ Q_2 & Q_3\end{bmatrix}\begin{bmatrix}\eta_7(t)\\ \dot{x}(s)\end{bmatrix} ds$$

which lead to $V_3(t) \geq 0$ for all $t \in [t_k, t_{k+1})$. Furthermore, the term $\int_{t_k-\tau}^{t-\tau} \dot{x}^T(s)Q_3\dot{x}(s)ds$ is vanished at $t = t_k$, i.e., $\lim_{t\to t_k^-} V_3(t) \geq V_3(t_k)$.

Next, the time derivatives of (13) are derived as follows:

$$\begin{aligned}
\dot{V}_1(t) &= 2x^T(t)P\dot{x}(t) + \eta_1^T(t)W\eta_1(t) \\
&\quad - \eta_1^T(t-\tau)W\eta_1(t-\tau) + \tau\dot{x}^T(t)S\dot{x}(t) \\
&\quad \underbrace{- \int_{t-\tau}^{t} \dot{x}^T(s)S\dot{x}(s)ds}_{:=T_1(t)} \qquad (14)
\end{aligned}$$

$$\begin{aligned}
&\dot{V}_2(t) \\
&= d_2(t)(2\dot{\eta}_2^T(t)X_1\eta_3(t) + 2\eta_2^T(t)X_1\dot{\eta}_3(t) + \eta_6^T U\eta_6) \\
&\quad + d_1(t)(2\dot{\eta}_4^T(t)X_2\eta_5(t) + 2\eta_4^T(t)X_2\dot{\eta}_5(t) - \eta_6^T U\eta_6) \\
&\quad - 2\eta_2^T(t)X_1\eta_3(t) + d_2(t)\dot{x}^T(t-\tau)R_1\dot{x}(t-\tau) \\
&\quad + 2\eta_4^T(t)X_2\eta_5(t) + d_1(t)\dot{x}^T(t-\tau)R_2\dot{x}(t-\tau) \\
&\quad \underbrace{- \int_{t_k-\tau}^{t-\tau} \dot{x}^T(s)R_1\dot{x}(s)ds}_{:=T_2(t)} \\
&\quad \underbrace{- \int_{t-\tau}^{t_{k+1}-\tau} \dot{x}^T(s)R_2\dot{x}(s)ds}_{:=T_3(t)} \qquad (15)
\end{aligned}$$

$$\begin{aligned}
\dot{V}_3(t) &= 2\tau_M\dot{\eta}_7(t)Q_1\eta_7(t) + 2\dot{x}^T(t-\tau)Q_2\eta_7(t) \\
&\quad + 2\big(x^T(t-\tau) - x^T(t_k-\tau)\big)Q_2\dot{\eta}_7(t) \\
&\quad + \dot{x}^T(t-\tau)Q_3\dot{x}(t-\tau). \qquad (16)
\end{aligned}$$

Then, since it clear that

$$\begin{aligned}
0 &\leq \int_{\alpha}^{\beta} \big(R\dot{x}(s) + M\eta(t)\big)^T R^{-1}\big(R\dot{x}(s) + M\eta(t)\big)ds \\
&= \int_{\alpha}^{\beta} \dot{x}^T(s)R\,\dot{x}(s)ds + (\beta-\alpha)\eta^T(t)M^T R^{-1}M\eta(t) \\
&\quad + 2\big(x^T(\beta) - x^T(\alpha)\big)M\eta(t)
\end{aligned}$$

the following inequality is satisfied

$$\begin{aligned}
T_1(t) &\leq \tau\eta_8^T(t)M^T S^{-1}M\eta_8(t) \\
&\quad + 2\big(x^T(t) - x^T(t-\tau)\big)M\eta_8(t) \qquad (17) \\
T_2(t) &\leq d_1(t)\eta_9^T(t)N_1^T R_1^{-1}N_1\eta_9(t) \\
&\quad + 2\big(x^T(t-\tau) - x^T(t_k-\tau)\big)N_1\eta_9(t) \qquad (18) \\
T_3(t) &\leq d_2(t)\eta_{10}^T(t)N_2^T R_2^{-1}N_2\eta_{10}(t) \\
&\quad + 2\big(x^T(t_{k+1}-\tau) - x^T(t-\tau)\big)N_2\eta_{10}(t). \qquad (19)
\end{aligned}$$

The following additional zero equalities holds:

$$0 = 2\eta_{11}^T(t)G^T\big(Ax(t) + BFx(t_k-\tau) - \dot{x}(t)\big). \quad (20)$$

Subsequently, by combining (14)-- (20), we can obtain

$$\dot{V}(t) \leq \eta^T(t)\Psi(t)\eta(t)$$

where

$$\begin{aligned}
\Psi(t) &= \Psi_1 + \Psi_2(t) + \tau\Xi_8^T M^T S^{-1}M\Xi_8 \\
&\quad + d_1(t)\Xi_9^T N_1^T R_1^{-1}N_1\Xi_9 + d_2(t)\Xi_{10}^T N_2^T R_2^{-1}N_2\Xi_{10}.
\end{aligned}$$

As a result, from $t \in [t_k, t_{k+1})$ and $h_k \in [h_m, h_M]$, the stability condition $\dot{V}(t) < 0$ can be represented as the following linear convex combination, for $h_k \in \{h_m, h_M\}$:

$$0 > \Psi_1 + \Psi_2(t_k) + \tau\Xi_8^T M^T S^{-1}M\Xi_8 + h_k\Xi_{10}^T N_2^T R_2^{-1}N_2\Xi_{10}^T$$
$$0 > \Psi_1 + \Psi_2(t_{k+1}) + \tau\Xi_8^T M^T S^{-1}M\Xi_8 + h_k\Xi_9^T N_1^T R_1^{-1}N_1\Xi_9$$

which are transformed into (11) and (12) using the Schur complement. ■

Based on the stability conditions established in Theorem 1, the sampled-data control gain is derived in the following theorem.

Theorem 2: For given positive scalars ε_1, ε_2, τ, h_m, and h_M, the closed-looped system (9) is asymptotically stable, if there exist matrices $0 < \bar{P} = \bar{P}^T \in \mathbb{R}^{n\times n}$, $0 < \bar{W} = \bar{W}^T \in \mathbb{R}^{2n\times 2n}$, $0 < \bar{S} = \bar{S}^T \in \mathbb{R}^{n\times n}$, $\bar{X}_1$, $\bar{X}_2 \in \mathbb{R}^{2n\times 3n}$, $\bar{R}_1 = \bar{R}_1^T$, $\bar{R}_2 = \bar{R}_2^T \in \mathbb{R}^{n\times n}$, $\bar{U} = \bar{U}^T \in \mathbb{R}^{2n\times 2n}$, $\bar{Q}_1 = \bar{Q}_1^T \in \mathbb{R}^{2n\times 2n}$, $\bar{Q}_2 \in \mathbb{R}^{n\times 2n}$, $\bar{Q}_3 = \bar{Q}_3^T \in \mathbb{R}^{n\times n}$, $\bar{G} \in \mathbb{R}^{n\times n}$, and $\bar{F} \in \mathbb{R}^{m\times n}$ such that the following conditions are satisfied, for $h_k \in \{h_m, h_M\}$:

$$0 < \begin{bmatrix}\bar{\mathrm{Q}}_1 & (*)\\ \bar{\mathrm{Q}}_2 & \bar{\mathrm{Q}}_3\end{bmatrix} \quad (21)$$

$$0 > \begin{bmatrix} \bar{\Psi}_1 + \bar{\Psi}_2(\mathrm{t_k}) & (*) & (*) \\ \tau\bar{M}\Xi_8 & -\tau\,\bar{S} & 0 \\ \mathrm{h_k}\bar{N}_2\Xi_{10} & 0 & -\mathrm{h_k}\bar{R}_2 \end{bmatrix} \quad (22)$$

$$0 > \begin{bmatrix} \bar{\Psi}_1 + \bar{\Psi}_2(\mathrm{t_{k+1}}) & (*) & (*) \\ \tau\bar{M}\Xi_8 & -\tau\,\bar{S} & 0 \\ \mathrm{h_k}\bar{N}_1\Xi_9 & 0 & -\mathrm{h_k}\bar{R}_1 \end{bmatrix} \quad (23)$$

where

$$\begin{aligned}\bar{\Psi}_1 &= He\{\boldsymbol{e}_1^T\bar{P}\boldsymbol{e}_7\} + \Xi_1^T\bar{W}\Xi_1 - \hat{\Xi}_1^T\bar{W}\hat{\Xi}_1 + \tau\boldsymbol{e}_7^T\bar{S}\boldsymbol{e}_7 \\ &\quad + He\{(\boldsymbol{e}_1^T - \boldsymbol{e}_2^T)\bar{M}\Xi_8 + (\boldsymbol{e}_2^T - \boldsymbol{e}_3^T)\bar{N}_1\Xi_9\} \\ &\quad + He\{(\boldsymbol{e}_4^T - \boldsymbol{e}_2^T)\bar{N}_2\Xi_{10} - \Xi_2^T\bar{X}_1\Xi_3 + \Xi_4^T\bar{X}_2\Xi_5\} \\ &\quad + He\{\Xi_{11}^T(A\bar{G}\boldsymbol{e}_1 + B\bar{F}\boldsymbol{e}_3 - \bar{G}\boldsymbol{e}_7) + \tau_M\bar{\Xi}_7^T\bar{Q}_1\Xi_7\} \\ &\quad + He\{\boldsymbol{e}_8^T\bar{Q}_2\Xi_7 + (\boldsymbol{e}_2^T - \boldsymbol{e}_3^T)\bar{Q}_2\bar{\Xi}_7 + \boldsymbol{e}_8^T\bar{Q}_3\boldsymbol{e}_8\} \\ \bar{\Psi}_2(t) &= d_2(t)He\{\bar{\Xi}_2^T\bar{X}_1\Xi_3 + \Xi_2^T\bar{X}_1\bar{\Xi}_3 + \Xi_6^T\bar{U}\Xi_6 + \boldsymbol{e}_8^T\bar{R}_1\boldsymbol{e}_8\} \\ &\quad + d_1(t)He\{\bar{\Xi}_4^T\bar{X}_2\Xi_5 + \Xi_4^T\bar{X}_2\bar{\Xi}_5 - \Xi_6^T\bar{U}\Xi_6 + \boldsymbol{e}_8^T\bar{R}_2\boldsymbol{e}_8\}\end{aligned}$$

Then, the control gain is reconstructed by

$$F = \bar{F}\bar{G}^{-1}. \quad (24)$$

Proof: Let us construct several congruent transformation matrices $0 < \bar{G} = \bar{G}^{-1}$, $\boldsymbol{G}_3 = I_3 \otimes \bar{G}$, and $\boldsymbol{G}_{10} = I_{10} \otimes \bar{G}$. Then, condition (21), (22) and (23) are derived by pre- and post-multiplying (10), (11) and (12) by $\boldsymbol{G}_3^T$, $\boldsymbol{G}_{10}^T$, and $\boldsymbol{G}_{10}^T$ and its transpose, respectively. ■

4. Numerical verification

In this section, the maximum allowable sampling interval and control gain are obtained by solving the LMI conditions in Theorem 2 using the LMI solver in the Robust Control Toolbox of MATLAB. Subsequently, the simulation results for the sampled-data control of the DC-DC DAB converter are obtained using PSIM software.

Table 1. *DAB DC-DC converter parameters*

Parameter	Symbol	Value
Input voltage	v_1	$100V$
Load resistance	R	50Ω
Phase-shifting inductance	L	$60\mu H$
Output capacitor	C	$220\mu F$
Switching frequency	f_s	$20kHz$
Transformer turns ratio	n	1

Table 2. *Comparison of maximized h_M for different τ*

Time delay	Sampling interval
$\tau = 1\mu s$	$h_M = 55\mu s$
$\tau = 10\mu s$	$h_M = 37\mu s$

Let us recall the DAB DC-DC converter system model (9) with the parameters are set as provided in Table 1. The values $\varepsilon_1 = 12.5$ and $\varepsilon_2 = 0.001$ were initially selected to guarantee the feasibility of the LMIs in Theorem 2 with $h_m = h_M = 1\mu s$. Subsequently, the h_M was incrementally increased by $1\mu s$ increments, while continuously verifying the feasibility of the LMI conditions. This procedure enabled the determination of the maximum allowable sampling interval alongside the control gain. Accordingly, Table 2 presents the maximum allowable sampling interval h_M of proposed controller corresponding to various values of the communication delay τ. In addition, for $\tau = 1\mu s$ and $h_M = 55\mu s$, the following control gain is provided by solving LMIs in Theorem 2:

$$F = [-0.0083 \;\; -0.0130].$$

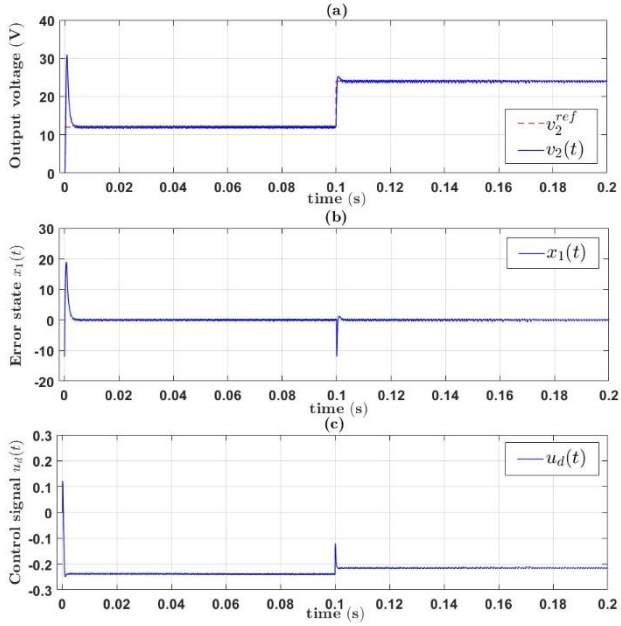

Figure 3. *Simulation results: (a) output voltage $v_2(t)$, (b) error state $x_1(t)$, and (c) control signal $u_d(t)$*

As a simulation results, when employing the proposed sampled-data controller with reference output voltage v_2^{ref} that steps up from $12V$ to $24V$ at $t = 0.1s$, the response of output voltage $v_2(t)$, error state $x_1(t)$, and control signal $u_d(t)$ are shown in Figure 3. It is revealed from Figure 3-(a) and (b) that the state error converges to zero as the output voltage approaches the reference value, demonstrating the stability and accuracy of the control system. Furthermore, Figure 3-(c) shows that the control input $u_d(t)$ varies according to the reference voltage and remains within the allowable range $u_d(t) \in [-0.25, 0.25]$, thereby satisfying the input constraint.

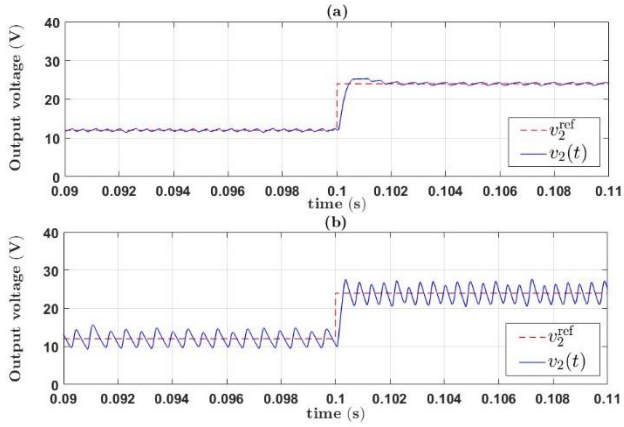

Figure 4. *Simulation results: (a) Sampled-data controller and (b) discrete-time controller*

Furthermore, to demonstrate the effectiveness of the proposed sampled-data controller for the DAB DC-DC

converter, its performance is compared with the discrete-time modeling approach (as described in [12]) in Figure 4. Notably, Figure 4 shows that the sampled-data controller achieves smoother tracking responses than the discrete-time controller. This comparison underscores the advantage of the proposed method, particularly as the sampling period increases, whereas the discrete-time controller exhibits considerable trajectory oscillations under the same conditions.

5. Conclusion

This study has presented the design of a sampled-data controller for a DAB DC-DC converter subject to communication delays. By incorporating an improved looped-functional approach alongside a discontinuous function into the stability analysis, the controller effectively exploits system state information obtained during sampling and transmission. Consequently, sufficient stabilization conditions were established in the form of LMIs. The simulation results validate the effectiveness of the proposed method in decreasing the sampling frequency, which consequently contributes to a reduction in implementation costs for both the controller and the communication network. In future research, we will focus on enhancing the robustness of the proposed approach with respect to modeling uncertainties and time delay variations.

REFERENCES

[1] A. N. Vargas, L. P. Sampaio, L. Acho, L. Zhang, and J. B. R. do Val, "Optimal control of DC–DC buck converter via linear systems with inaccessible Markovian jumping modes", *IEEE Transactions on Control Systems Technology,* vol. 24, no. 5, pp. 1820–1827, 2016. https://doi.org/10.1109/TCST.2015.2508959

[2] M. Tavan, K. Sabahi, A. Hajizadeh, M. N. Soltani, and K. Jessen, "Overcoming the detectability obstacle in adaptive output feedback control of DC–DC boost converter with unknown load", *IEEE Transactions on Control Systems Technology,* vol. 29, no. 6, pp. 2678–2686, 2021. https://doi.org/10.1109/TCST.2020.3044378

[3] X.-M. Zhang, Q.-L. Han, and B.-L. Zhang, "An overview and deep investigation on sampled-data-based event-triggered control and filtering for networked systems", *IEEE Transactions on Industrial Informatics,* vol. 13, no. 1, pp. 4–16, 2017. https://doi.org/10.1109/TII.2016.2607150

[4] E. Fridman, "A refined input delay approach to sampled-data control", *Automatica,* vol. 46, no. 2, pp. 421–427, 2010. https://doi.org/10.1016/j.automatica.2009.11.017

[5] A. Seuret, "A novel stability analysis of linear systems under asynchronous samplings", *Automatica,* vol. 48, no. 1, pp. 177–182, 2012. https://doi.org/10.1016/j.automatica.2011.09.033

[6] T. H. Lee and J. H. Park, "Stability analysis of sampled-data systems via free-matrix-based time-dependent discontinuous Lyapunov approach", *IEEE Transactions on Automatic Control,* vol. 62, no. 7, pp. 3653–3657, 2017. https://doi.org/10.1109/TAC.2017.2670786

[7] H.-B. Zeng, K. L. Teo, and Y. He, "A new looped-functional for stability analysis of sampled-data systems", *Automatica,* vol. 82, pp. 328–331, 2017. https://doi.org/10.1016/j.automatica.2017.04.051

[8] L. Shi, W. Lei, Z. Li, J. Huang, Y. Cui, and Y. Wang, "Bilinear discrete-time modeling and stability analysis of the digitally controlled dual active bridge converter", *IEEE Transactions on Power Electronics,* vol. 32, no. 11, pp. 8787–8799, 2017. https://doi.org/10.1109/TPEL.2016.2640659

[9] A. Tong, L. Hang, H. S. Chung, and G. Li, "Using sampled-data modeling method to derive equivalent circuit and linearized control method for dual-active-bridge converter", *IEEE Journal of Emerging and Selected Topics in Power Electronics,* vol. 9, no. 2, pp. 1361–1374, 2021. https://doi.org/10.1109/JESTPE.2019.2961138

[10] M. T. Iqbal and A. I. Maswood, "An explicit discrete-time large and small-signal modeling of the dual active bridge DC–DC converter based on the time scale methodology", *IEEE Journal of Emerging and Selected Topics in Industrial Electronics,* vol. 2, no. 4, pp. 545–555, 2021. https://doi.org/10.1109/JESTIE.2021.3087942

[11] Y. Zhu *et al*., "Model predictive control with a novel parameter identification scheme for dual-active-bridge converters", *IEEE Journal of Emerging and Selected Topics in Power Electronics,* vol. 11, no. 5, pp. 4704–4713, 2023. https://doi.org/10.1109/JESTPE.2023.3289299

[12] N. N. Nam and S. H. Kim, "Robust tracking control of dual-active-bridge DC–DC converters with parameter uncertainties and input saturation", *Mathematics,* vol. 10, no. 24, Art. no. 4719, 2022. https://doi.org/10.3390/math10244719